Measurement of Energy Transfer Time in Colloidal Mn-Doped Semiconductor Nanocrystals

Hsiang-Yun Chen, Tai-Yen Chen, and Dong Hee Son*

Department of Chemistry, Texas A&M University, College Station, Texas 77842

Received: January 13, 2010; Revised Manuscript Received: February 4, 2010

The exciton−dopant energy transfer time in colloidal Mn-doped CdS/ZnS core/shell nanocrystals was investigated via pump−probe transient absorption measurements. The energy transfer time was obtained from the comparative analysis of the dynamics of exciton relaxation in undoped and doped nanocrystal samples with well-defined doping radius and concentration. For this purpose, the transient absorption was measured in the near-IR region probing primarily intraband transition of excitons without signal saturation even at high exciton densities, which is particularly useful for studying the energy transfer in a wide range of exciton densities. With an increasing Mn doping concentration, exciton-dopant energy transfer became faster, effectively competing with both radiative and nonradiative relaxation of exciton. In the spherical Mn-doped CdS/ZnS core/shell nanocrystals studied here, the time scale of energy transfer between a single pair of exciton and Mn^{2+} ion was determined to be ∼60 ps.

1. Introduction

Semiconductor nanocrystals doped with paramagnetic transition metal ions, such as Mn-doped CdS nanocrystals, possess unique optical and magnetic properties distinct from their undoped counterparts that arise from the interaction of exciton with dopant ions.[1–4] For instance, the doped Mn^{2+} ions can function as an efficient and long-lived sensitized energy reservoir for the excitons created in semiconductor host matrix via energy transfer from exciton to the ligand field state of Mn^{2+} ions.[5,6] The energy transfer from exciton to dopant ions is essentially an intersystem crossing and results in strong phosphorescence emission from the ligand field transition of dopant ions.[4] In Mn-doped II−VI semiconductor nanocrystals, phosphorescence of Mn^{2+} occurs near 600 nm with a lifetime of $\sim 10^{-3}$ s.[4,7,8] Due to the significant spatial overlap of the exciton and dopant wave functions in the confined space of the nanocrystals, the energy of exciton can be rapidly transferred to Mn^{2+} ions competing with both radiative and nonradiative exciton relaxation pathways.[4,9] For this reason, Mn-doped semiconductor nanocrystals often exhibit a superior luminescence quantum yield than undoped counterparts making them attractive for many applications.[10–12]

Many earlier studies investigated the mechanisms of energy transfer and static and dynamic phosphorescence from Mn^{2+} ions resulting from the energy transfer.[5,9,13,14] However, the rate of energy transfer from exciton to Mn^{2+} ions, a key factor determining the effectiveness of Mn-doped nanocrystals as the sensitized energy reservoir, has been investigated much less. Earlier studies employing time-resolved emission and transient absorption suggested the exciton−Mn energy transfer time is in the range of several tens to hundreds of picoseconds in colloidal Mn-doped nanocrystals.[15,16] However, difficulties in controlling the doping site and complications arising from the multiple emitting species (e.g., free and trapped exciton) posed challenges in obtaining a quantitative understanding of the energy transfer time.

Recently, studies on the radial doping position-dependent Mn luminescence intensity in Mn-doped CdS/ZnS nanocrystals showed that the quantum yield of Mn luminescence increases as the doping position gets closer to the center of the nanocrystal.[9] This result is consistent with the predictions from the possible energy transfer mechanisms (Förster-, Dexter-, or Auger-like mechanism),[4,9,13] while the exact energy transfer mechanism is still not entirely clear. The energy transfer rate could not be obtained, however, from this steady-state quantum yield measurement due to uncertainties in the rates of other competing nonradiative processes.

In this report, we describe the time-resolved measurement of the energy transfer in Mn-doped CdS/ZnS core/shell nanocrystals with well-defined doping radius and concentration, which will enable the correlated study of the energy transfer rate and the structure of the doped nanocrystals. To obtain information on the time scale of the energy transfer, we compared the exciton relaxation dynamics in Mn-doped and undoped nanocrystals as a function of Mn doping concentration at a known fixed radial doping position. The transient absorption signal from the photoexcited exciton decayed faster with the increase of Mn doping concentration due to the energy transfer. The energy transfer rate was linear to the Mn doping concentration at the average exciton density of 1 per particle. This allowed us to extract the energy transfer time for a single pair of exciton and Mn^{2+} ion at a given radial doping position. Exciton relaxation dynamics were obtained by probing at the near-IR region, where the transient absorption signal is primarily attributed to the intraband transition of excitons. Near-IR probing has an advantage over visible probing of interband exciton absorption since the transient absorption signal at near-IR increases linearly with exciton density within a wide range of exciton densities without saturation or cancellation of the signal. Transient absorption data of the nanocrystals with varying Mn doping concentrations (2−13 Mn^{2+} ions per particle) were analyzed to extract the energy transfer time with a simple kinetic model, where the energy transfer competes with exciton relaxation and trapping at the rate proportional to Mn doping concentration. The strategy to obtain a quantitative energy transfer time in Mn-doped semiconductor nanocrystals with a well-defined doping radius and concentration described here will be useful in obtaining a quantitative understanding of the

* To whom correspondence should be addressed. E-mail: dhson@mail.chem.tamu.edu. Phone: 979-458-2990.

10.1021/jp100352m
Published on Web 02/17/2010

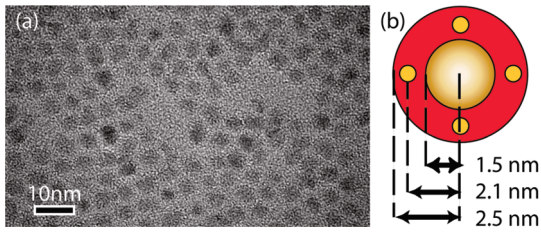

Figure 1. (a) TEM image of Mn-doped CdS/ZnS nanocrystals. (b) Dimensions of Mn-doped CdS/ZnS core/shell nanocrystals. CdS core radius and ZnS shell thickness is 1.5 and 1 nm, respectively. Mn^{2+} ions are doped at $r = 2.1$ nm.

correlation between the doping structure of the nanocrystals and the rate of energy transfer.

2. Experimental Section

Material Preparation and Characterization. To investigate the rate of exciton−dopant energy transfer, we used spherical colloidal Mn-doped CdS/ZnS core/shell nanocrystals where Mn^{2+} ions are radially doped at a known distance from the center of the nanocrystals. Colloidal Mn-doped CdS/ZnS core/shell nanocrystals were prepared by following the published procedure and its variations.[17,18] Initially, CdS core was synthesized using sulfur and cadmium oxide as the precursors in the mixture of 1-octadecene (ODE) and oleic acid at 250 °C. On the surface of CdS core, ZnS shell was coated layer-by-layer by alternately adding the solutions of sulfur and zinc stearate until the desired number of ZnS layers were coated. Subsequently, a solution mixture of sulfur and manganese acetate tetrahydrate in oleylamine and ODE was added at 260 °C in order to form the Mn-doped layer on the surface of the CdS/ZnS nanocrystal. Finally, additional layers of ZnS were coated following the same procedure described above. After each step, the size of the nanocrystals was characterized by transmission electron microscope (TEM). The average diameter of the Mn-doped CdS/ZnS nanocrystals determined from TEM was 5.1 nm with CdS core diameter of 3 nm. Mn^{2+} ions were doped at 2.1 nm from the center of the nanocrystals (Figure 1). In all the undoped and doped nanocrystals, the diameter of CdS core, thickness of ZnS shell, and Mn doping position were kept identical.

The average number of Mn^{2+} ions per particle, $\langle n_{Mn} \rangle$, was measured from the elemental analysis employing inductively coupled plasma mass spectrometry (ICP-MS). In this work, nanocrystal samples with $\langle n_{Mn} \rangle = 0$, 2, 3, 4, and 13 were prepared. Absorption and emission spectra of the undoped and Mn-doped CdS/ZnS nanocrystals are shown in Figure 2a. The absorption spectra of the nanocrystals with different $\langle n_{Mn} \rangle$ are very similar, which further indicates the uniformity of the core size and shell thickness of all the nanocrystal samples. Photoluminescence spectra of all four samples were measured with 370 nm excitation. The lifetime of Mn phosphorescence measured with nanosecond-pulsed excitation at 337 nm from N_2 laser was in the range of 1−4 ms and it decreased with increasing $\langle n_{Mn} \rangle$ as shown in Figure 2b. The intensity of Mn phosphorescence increased with a concomitant decrease of band-edge exciton fluorescence as $\langle n_{Mn} \rangle$ increased at low doping concentrations. A small amount of red-shift of Mn phosphorescence with increasing $\langle n_{Mn} \rangle$, ascribed to Mn−Mn exchange interaction, is consistent with the previously reported observations.[14,19]

Pump−Probe Measurement of Energy Transfer Time. To measure the time scale of exciton−dopant energy transfer, we employed pump−probe transient absorption spectroscopy. The

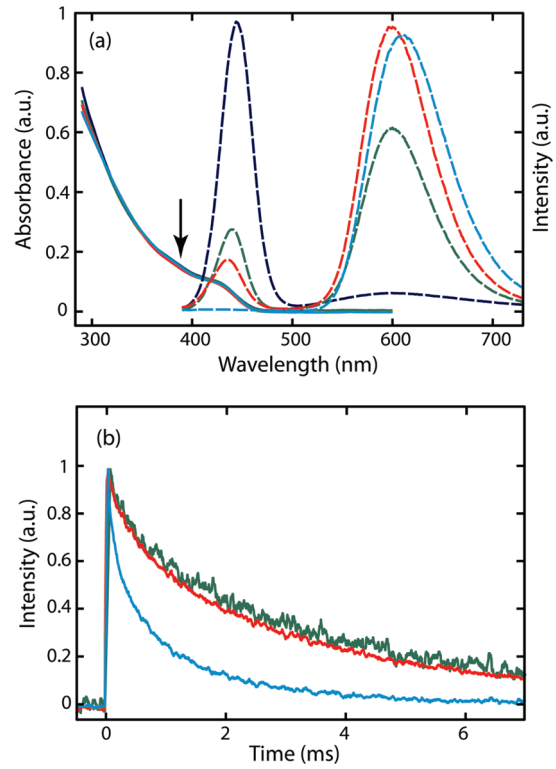

Figure 2. (a) Absorption (solid) and emission spectra (dashed) of Mn-doped CdS/ZnS core/shell nanocrystals with different Mn doping levels. $\langle n_{Mn} \rangle = 0$ (blue), 2 (green), 3 (red), and 13 (cyan). The arrow indicates the pump wavelength for transient absorption measurements. (b) Time dependent Mn phosphorescence intensity following 337 nm excitation. $\langle n_{Mn} \rangle = 2$ (green), 3 (red), and 13 (cyan).

energy transfer time was extracted from the comparison of the rate of exciton relaxation in doped and undoped semiconductor nanocrystals using a simple kinetic model, where Mn-doped nanocrystals have an additional exciton relaxation pathway, i.e., exciton−dopant energy transfer. The transient absorption was measured with an amplified Titanium:Sapphire laser system operating at 3 kHz repetition rate. The pump beam centered at 390 nm was generated by doubling 60 fs, 780 nm fundamental output in a 300 μm-thick BBO (β-barium borate) crystal. The average fluence of the pump beam under the probe beam area was varied in the range of 0.9−24 mJ/cm^2 by using a combination of a half-wave plate and a polarizer. White light continuum, generated in 1 mm-thick sapphire or CaF_2 crystal by focusing several μJ of a 780 nm beam, was used as the probe source. The wavelength of the probe beam was preselected before the sample by placing a narrow slit in the beam path of the prism dispersion compensator. The time resolution of the measurement was ~100 fs based on instrument limited signal rise time. The fwhm (full width at half-maximum) beam size of the 390 nm pump and continuum probe beam was measured to be 300 and 30 μm, respectively. The sample solution (25 mL in total volume) was circulated as a free streaming jet (400 μm thick) at a linear speed of several meters/second to avoid reexcitation of the same sample region before the complete relaxation of Mn^{2+} ligand field excited state and potential photodamage of the sample. The average number of photoexcited excitons (i.e., the number of 390 nm photons absorbed) per particle at a given excitation fluence was estimated from the energy of the absorbed pump beam by the sample within the area of the probe beam and the concentration of the nanocrystals. The concentration of the nanocrystals (21 μM) was determined from the average diameter of the nanocrystals

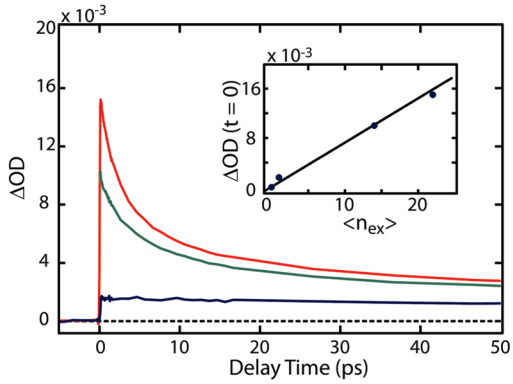

Figure 3. Transient absorption data of undoped CdS/ZnS core/shell nanocrystals under various exciton densities obtained with 390 nm pump and 880 nm probe. Blue, green, and red lines are for $\langle n_{ex} \rangle = 1$, 14, and 22, respectively. The inset displays the peak amplitude of ΔOD data vs $\langle n_{ex} \rangle$.

measured from TEM and total metal ion concentration measured from elemental analysis employing ICP mass spectrometry. The detailed procedure for the estimation of the photoexcited exciton density is described in the Supporting Information.

3. Results and Discussion

To extract the energy transfer time from the comparison of the dynamics of exciton relaxation in undoped and doped nanocrystals, we obtained transient absorption data of CdS/ZnS nanocrystals with varying doping concentrations. When investigating the dynamics of exciton relaxation of CdS or CdSe nanocrystals from transient absorption measurements, typically the bleach signal of the band-edge exciton absorption in the visible spectral region is monitored at low exciton densities, e.g., less than one exciton per particle.[20–23] At higher exciton densities, however, the bleach signal saturates and can even be partially masked by an absorptive contribution arising from multiexciton interaction or trapped exciton.[24,25] This limits the usefulness of probing the bleach of interband exciton transition as a way to monitor the exciton relaxation dynamics to the low exciton density region. On the other hand, the pump-induced absorption in the near-IR region significantly below the bandgap does not suffer from the saturation of the bleach signal or cancellation of bleach by other absorptive signals. Furthermore, the initial amplitude of the pump-induce absorption near zero time delay increases more linearly to the exciton density within a wide range of exciton densities.[26] Therefore, monitoring the pump-induced absorption at the near-IR region can be more useful when the examination of the exciton relaxation dynamics in a wide range of exciton densities is required.

In this study, all the transient absorption (ΔOD) data were obtained at the probe wavelength of 880 nm (1.4 eV), lower in energy than the band-edge absorption of the undoped and Mn-doped CdS/ZnS nanocrystals investigated in this work (2.9 eV). Figure 3 shows ΔOD data of undoped CdS/ZnS core/shell nanocrystals probed at 880 nm at the average exciton densities of $\langle n_{ex} \rangle = 1$, 14, and 22 per particle. ΔOD data probed at other near-IR wavelengths in the 700−900 nm range were similar to the data obtained at 880 nm, indicating that the induced absorption in this region has a relatively flat spectral feature (Supporting Information, Figure S2). The comparison of ΔOD at zero time delay for the case of $\langle n_{ex} \rangle = 1$ (ΔOD < 0.002) in Figure 3 and the linear absorption spectrum of the nanocrystal sample shown in Figure 2a indicates that the transition probed at near-IR is more than an order of magnitude weaker than interband exciton transition (e.g., OD = 0.1 at $\lambda = 420$ nm). The pump-induced absorption in this spectral region was previously interpreted as the intraband absorption of the exciton.[26] While the assignment of the absorption at 880 nm is more complex than the spectroscopic features in the visible or mid-IR region more readily associated with a particular inter- or intraband transition, the dynamics at 880 nm can be interpreted as the relaxation of the excited excitons in an averaged sense.[26] Therefore, the dynamics of exciton relaxation reflected in ΔOD data of this study represent the collective dynamics of all the excitons rather than the relaxation of the band-edge exciton only.

In Figure 3, the peak amplitude of ΔOD data near zero time delay increases near-linearly with the exciton density as shown in the inset. This linearity of the signal to the exciton density allows us to monitor the exciton relaxation dynamics within a broad range of exciton densities. The highly multiexponential feature of the dynamics at higher exciton densities can be explained with Auger relaxation of excitons.[27,28] The accurate modeling of ΔOD data in Figure 3, especially at higher exciton densities, is somewhat complex. It requires information on all the radiative and nonradiative exciton relaxation pathways (e.g., trapping of exciton) and absorption cross sections of all the processes resonant at the probe wavelength, which are not always unambiguous. However, information on the time scale of exciton−dopant energy transfer can be obtained from the comparative analysis of ΔOD data, since the energy transfer is manifested in the "difference" of the exciton relaxation dynamics of doped and undoped nanocrystals. At lower exciton densities (e.g., $\langle n_{ex} \rangle \approx <1$), such comparative analysis is more straightforward since the dynamics of exciton relaxation is simpler without highly nonlinear Auger relaxation.

Built upon the robustness of transient near-IR absorption as the probe for the exciton relaxation dynamics as discussed above, we first investigated the energy transfer time at the average exciton density of $\langle n_{ex} \rangle = 1$. To extract the time scale of exciton−dopant energy transfer from the comparative analysis of exciton relaxation dynamics, we measured ΔOD of Mn-doped CdS/ZnS nanocrystals with varying Mn doping concentration. Figure 4a compares ΔOD data of the undoped and doped nanocrystals with $\langle n_{Mn} \rangle = 3$, 13 probed at 880 nm at the average exciton density of $\langle n_{ex} \rangle = 1$. The decay of ΔOD can be fit to one or two exponential functions. The amplitude of ΔOD at zero time delay is not very sensitive to Mn doping concentration $\langle n_{Mn} \rangle$, which indicates that a common spectroscopic process is probed in all nanocrystal samples. Such independence of ΔOD at zero time delay on $\langle n_{Mn} \rangle$ was maintained at higher exciton densities as will be shown later, further demonstrating the usefulness of near-IR probe (see Figure 6). When ΔOD data are measured in visible region ($\lambda = 455$ nm) near the band-edge exciton transition, on the other hand, the bleach signal at zero time delay exhibits a signature of an absorptive component partially canceling the bleach signal especially in the sample with a high level of Mn doping (see the Supporting Information, Figure S3). This also makes near-IR probing of intraband transition more attractive for the study of exciton−dopant energy transfer.

In Figure 4a, the time scale of the fast decaying component in ΔOD data becomes shorter as $\langle n_{Mn} \rangle$ increases. We attribute the increasingly faster decay of ΔOD with increasing $\langle n_{Mn} \rangle$ to the energy transfer from exciton to Mn^{2+} ions. To extract the time scale of the energy transfer, we first employed a simple subtractive procedure without fitting the data to a detailed kinetic model with all the radiative and nonradiative exciton relaxation

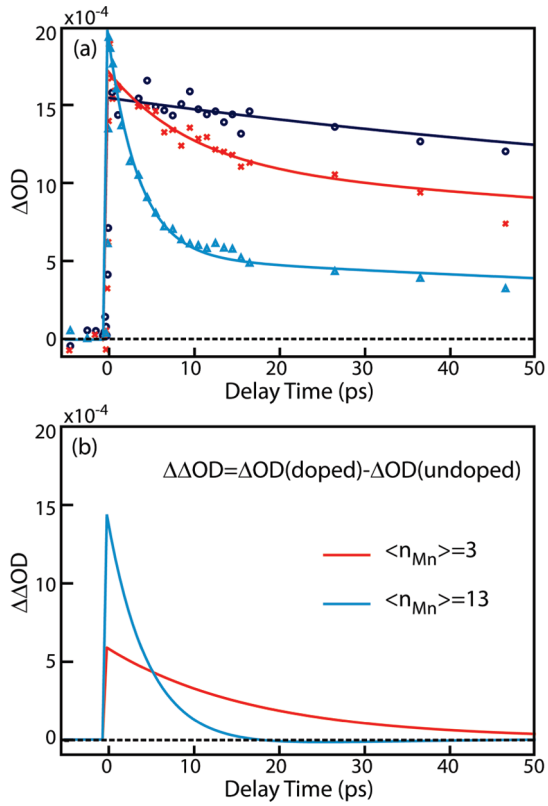

Figure 4. (a) Transient absorption data of undoped and Mn-doped CdS/ZnS nanocrystals obtained with 390 nm pump and 880 nm probe at $\langle n_{ex} \rangle = 1$. Experimental data (symbol) and fit to exponential functions (solid line) are shown for $\langle n_{Mn} \rangle = 0$ (blue), 3 (red), and 13 (cyan). (b) ΔΔOD data of $\langle n_{Mn} \rangle = 3$ and 13 samples.

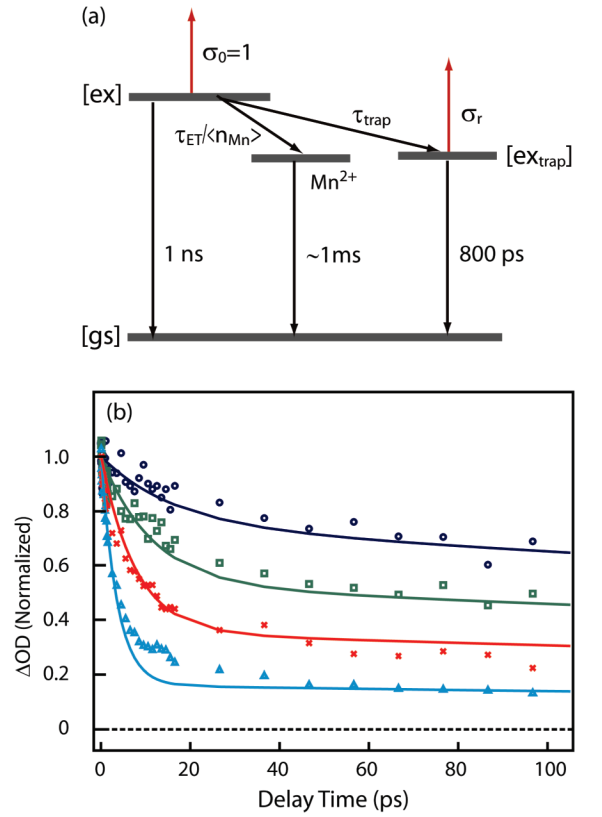

Figure 5. (a) Kinetic scheme used for modeling of energy transfer competing with radiative and nonradiative relaxation (trapping) of exciton in Mn-doped CdS/ZnS nanocrystals. [gs], [ex], and [ex_{trap}] represent ground state, excited state (exciton), and trapped excited state (trapped exciton). The fitting parameters are τ_{ET}, τ_{trap}, and σ_r. See the text. (b) Experimental data (symbol) and fit (solid line) of the data to the kinetic model. $\langle n_{Mn} \rangle = 0$ (blue), 2 (green), 4 (red), and 13 (cyan).

pathways. Figure 4b displays the difference between the two ΔOD data (ΔΔOD) from the doped and undoped nanocrystal samples, where the subtraction was performed after normalizing the data to the amplitude of the slowly decaying component that has the time constant of ~800 ps. This procedure is sufficient for obtaining a rough time scale of the energy transfer since ΔOD of undoped nanocrystals decays at a much slower rate compared to the time scale of the fast decaying component in ΔOD of doped nanocrystals. We interpret the time scale of the decay of ΔΔOD as the energy transfer time from exciton to dopant states for a given Mn^{2+} concentration. From the fit to a single exponential function, 18 and 4 ps were obtained for $\langle n_{Mn} \rangle = 3$ and 13, respectively. The ratio of the two times is close to the ratio of $\langle n_{Mn} \rangle$, which is expected from the first order energy transfer kinetics between an exciton and multiple Mn^{2+} ions. Extrapolation of the energy transfer time to the case of $\langle n_{Mn} \rangle = 1$ yields $\tau_{ET} = \sim 53$ ps for a single pair of exciton and Mn^{2+} ion in our CdS/ZnS core/shell nanocrystals at the doping radius of 2.1 nm. According to the earlier studies on bulk Mn-doped semiconductors and self-assembled Mn-doped quantum dots, the energy transfer between the exciton and dopant occurred on the time scale of tens of picoseconds.[29,30] In colloidal Mn-doped nanocrystals, Chung et al. reported 700 ps energy transfer time in aqueous colloidal solution of 2% Mn-doped ZnS nanocrystals from the comparison of the decay time of exciton emission and rise time of $^4T_1$ (Mn^{2+}) absorption at an unspecified exciton density.[15] Olano et al. observed the difference in transient absorption data between undoped and Mn-doped ZnSe nanocrystals, which exhibited the presence of an energy transfer channel in doped nanocrystal with the time constants of tens of picoseconds.[16] Although the direct comparison cannot be made between our and earlier measurements due to the uncertainties in the effective doping density and donor−acceptor distance in the earlier works, the time scales of the energy transfer are of the same order of magnitude except for Chung et al.'s work.

While the above analysis offers a simple way to obtain the approximate time scale of the energy transfer, it does not account for some detailed features in ΔOD data. For instance, a persistent and slowly decaying component ($\tau = \sim 800$ ps) in ΔOD data, whose amplitude decreases with increasing $\langle n_{Mn} \rangle$, is ignored in the analysis. One possible explanation for the slowly decaying component is the absorption from the trapped exciton.[25] According to the earlier studies in CdS and CdSe nanocrystals, electron and hole trapping was considered to occur on the times scale of sub picosecond to tens of picoseconds depending on the size and surface passivation of the nanocrystals.[22,24,25] Since the trapping will localize the wave function of electron or (and) hole at the defect site and lower the energy of exciton, the energy transfer from trapped exciton to Mn^{2+} ions will be inefficient. If the trapped exciton has an absorption at the probe wavelength, competition between the energy transfer and exciton trapping can explain the observed slowly decaying component in ΔOD data, whose amplitude decreases with increasing $\langle n_{Mn} \rangle$.

To extract the more refined energy transfer time taking into account the competition between the energy transfer and trapping, we fitted ΔOD data of Mn-doped nanocrystals of four different $\langle n_{Mn} \rangle$ to the kinetic model shown in Figure 5a. Three parameters, τ_{ET}, τ_{tr}, and σ_r, were optimized in the fitting. τ_{ET}

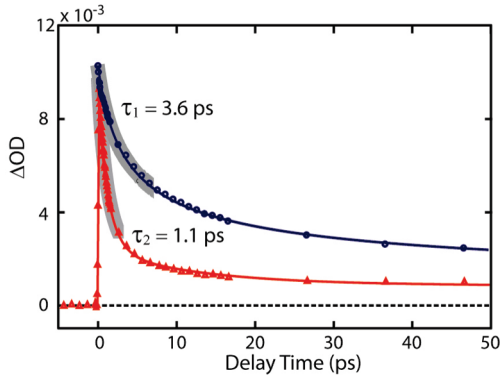

Figure 6. Transient absorption data of undoped and Mn-doped CdS/ZnS core/shell nanocrystals with $\langle n_{ex} \rangle = 14$. Experimental data (symbol) and fit (solid lines) are shown for $\langle n_{Mn} \rangle = 0$ (blue) and 13 (red). The time constants τ_1 and τ_2 were obtained from multiexponential fitting of the data.

and τ_{tr} represent the energy transfer time between a pair of exciton and Mn^{2+} ion and exciton trapping time, respectively. σ_r is the absorption cross section of the trapped exciton relative to the initially excited exciton. All four normalized ΔOD data were simultaneously fitted to $\Delta OD(t) = [ex](t) + \sigma_r[ex_{trap}](t)$ with the initial condition of $[ex](0) = 1$, where $[ex](t)$ and $[ex_{trap}](t)$ are the population of the initially excited and trapped exciton state at time t, respectively. Here, the apparent time scale of the energy transfer was assumed to be linear to $\langle n_{Mn} \rangle$. Since the fitting of the data and the optimized parameters are very insensitive to the decay times of [ex] and $[ex_{trap}]$ that account for the slowly decaying component on ~1 ns time scale, we used the fixed time constants for these processes. In fact, the extracted rate parameters vary only 3% when the time constants for the decay of [ex] and $[ex_{trap}]$ were varied from 1 to 10 ns.

Figure 5b shows the fitting result with optimized parameters of $\tau_{ET} = 60$ ps, $\tau_{tr} = 17$ ps, and $\sigma_r = 0.75$. With the inclusion of exciton trapping time and the absorption of trapped exciton as the additional parameters, the amplitude of the slow-decaying component is reasonably well reproduced for all four Mn doping concentrations. The value of τ_{ET} extracted from this more refined analysis is not significantly different from the value obtained from the analysis shown in Figure 4, suggesting that the simple subtractive analysis can also capture the approximate time scale of the energy transfer. It is interesting to note that the optimized trapping time (τ_{tr}) is within the range of electron and hole trapping times from earlier works on CdS and CdSe nanocrystals.[22,25] While the data from our study are insufficient to unambiguously determine the nature of trapping and the absorption from trapped exciton, the model works well for the purpose of extracting the time scale of the energy transfer.

To further examine the possibility of extending near-IR probe to study the time scale of the energy transfer at higher exciton densities, we measured ΔOD at higher excitation fluences corresponding to $\langle n_{ex} \rangle = 14$. ΔOD data of undoped and Mn-doped ($\langle n_{Mn} \rangle = 13$) nanocrystals are compared in Figure 6, where the doped nanocrystals exhibit the faster decay of the signal. In fact, the faster decay of ΔOD with increasing $\langle n_{Mn} \rangle$ was observed as a general trend (see the Supporting Information, Figure S4). Modeling the decay of ΔOD signal at higher exciton density and extracting the energy transfer time is, however, more complex than the low exciton density case due to the highly nonlinear Auger relaxation kinetics.

Here, we make a simple comparison of the exponential decay times at early delay time (<10 ps) only without attempting to make a detailed kinetic analysis. In Figure 6, the exponential time constants in the shaded regions are 3.6 and 1.1 ps carrying about 50% and 70% of the amplitude for undoped and doped ($\langle n_{Mn} \rangle = 13$) nanocrystal samples, respectively. Treating these time constants as the first-order time constants, one obtains an approximate time constant of 1.6 ps for the additional first-order process in the doped nanocrystal that can be ascribed to the energy transfer.[31] This can be crudely interpreted as $\tau_{ET} = 20$ ps for a single Mn^{2+} ion at this excitation condition. This suggests that despite the fast Auger relaxation of excitons at higher exciton densities, the energy transfer is sufficiently fast to compete with Auger relaxation. More detailed discussion on the measurement and analysis of energy transfer at higher exciton densities will be made in a future report.

4. Conclusions

In conclusion, exciton−dopant energy transfer time in Mn-doped CdS/ZnS core/shell nanocrystals was measured employing pump−probe transient absorption technique. By using the nanocrystals with well-defined doping radius and concentration, a quantitative energy transfer time that can be correlated with the doping structure of the nanocrystals was obtained. Energy transfer time was measured from the comparative analysis of the exciton relaxation dynamics in doped and undoped nanocrystals. For this purpose, a near-IR probe monitoring primarily the intraband transition of excitons was used. By employing a simple kinetic model, where the energy transfer competes with exciton relaxation and trapping, the energy transfer time of 60 ps for a pair of exciton and Mn^{2+} ion was obtained for 5.1 nm Mn-doped CdS/ZnS nanocrystals with doping radius of 2.1 nm and exciton density of 1 per particle. The strategy taken in this work will be useful in future studies on the relationship between the energy transfer time and structure of the doped nanocrystals.

Acknowledgement. .

This work was supported by the Welch Foundation (Grant No. A-1639). We thank Microscopy and Imaging Center, Materials Characterization Facility, and Elemental Analysis Laboratory of Texas A&M University for TEM, UV−Vis, photoluminescence, and ICP-MS measurements.

Supporting Information Available: Details of experimental setup and estimation of excitation density and additional transient absorption data with varying probing wavelengths and Mn doping concentrations. This material is available free of charge via the Internet at http://pubs.acs.org.

References and Notes

(1) Norris, D. J.; Efros, A. L.; Erwin, S. C. *Science* **2008**, *319*, 1776.
(2) Bacher, G.; Schömig, H.; Welsch, M. K.; Zaitsev, S.; Kulakovskii, V. D.; Forchel, A.; Lee, S.; Dobrowolska, M.; Furdyna, J. K.; König, B.; Ossau, W. *Appl. Phys. Lett.* **2001**, *79*, 524.
(3) Bacher, G.; Schömig, H.; Scheibner, M.; Forchel, A.; Maksimov, A. A.; Chernenko, A. V.; Dorozhkin, P. S.; Kulakovskii, V. D.; Kennedy, T.; Reinecke, T. L. *Phys. E* **2005**, *26*, 37.
(4) Beaulac, R.; Archer, P. I.; Ochsenbein, S. T.; Gamelin, D. R. *Adv. Funct. Mater.* **2008**, *18*, 3873.
(5) Bol, A. A.; Meijerink, A. *Phys. Rev. B* **1998**, *58*, R15997.
(6) Beaulac, R.; Archer, P. I.; van Rijssel, J.; Meijerink, A.; Gamelin, D. R. *Nano Lett.* **2008**, *8*, 2949.
(7) Ishizumi, A.; Jojima, E.; Yamamoto, A.; Kanemitsu, Y. *J. Phys. Soc. Jpn.* **2008**, *77*, 053705.
(8) Gan, C.; Zhang, Y.; Battaglia, D.; Peng, X.; Xiao, M. *Appl. Phys. Lett.* **2008**, *92*, 241111.
(9) Yang, Y.; Chen, O.; Angerhofer, A.; Cao, Y. C. *Chem.—Eur. J.* **2009**, *15*, 3186.
(10) Pradhan, N.; Goorskey, D.; Thessing, J.; Peng, X. *J. Am. Chem. Soc.* **2005**, *127*, 17586.

(11) Norris, D. J.; Yao, N.; Charnock, F. T.; Kennedy, T. A. *Nano Lett.* **2001**, *1*, 3.
(12) Thakar, R.; Chen, Y.; Snee, P. T. *Nano Lett.* **2007**, *7*, 3429.
(13) Nawrocki, M.; Rubo, Y. G.; Lascaray, J. P.; Coquillat, D. *Phys. Rev. B* **1995**, *52*, R2241.
(14) Suyver, J. F.; Wuister, S. F.; Kelly, J. J.; Meijerink, A. *Phys. Chem. Chem. Phys.* **2000**, *2*, 5445.
(15) Chung, J. H.; Ah, C. S.; Jang, D.-J. *J. Phys. Chem. B* **2001**, *105*, 4128.
(16) Olano, E. M.; Grant, C. D.; Norman, T. J.; Castner, E. W.; Zhang, J. Z. *J. Nanosci. Nanotechnol.* **2005**, *5*, 1492.
(17) Yu, W. W.; Peng, X. *Angew. Chem., Int. Ed.* **2002**, *41*, 2368.
(18) Yang, Y.; Chen, O.; Angerhofer, A.; Cao, Y. C. *J. Am. Chem. Soc.* **2006**, *128*, 12428.
(19) Vink, A. P.; de Bruin, M. A.; Roke, S.; Peijzel, P. S.; Meijerink, A. *J. Electrochem. Soc.* **2001**, *148*, E313.
(20) Klimov, V. I.; McBranch, D. W. *Phys. Rev. Lett.* **1998**, *80*, 4028.
(21) Guyot-Sionnest, P.; Shim, M.; Matranga, C.; Hines, M. *Phys. Rev. B* **1999**, *60*, R2181.
(22) Klimov, V. I. *J. Phys. Chem. B* **2000**, *104*, 6112.
(23) Burda, C.; Link, S.; Mohamed, M. B.; El-Sayed, M. *J. Chem. Phys.* **2002**, *116*, 3828.
(24) Sewall, S. L.; Cooney, R. R.; Anderson, K. E. H.; Dias, E. A.; Sagar, D. M.; Kambhampati, P. *J. Chem. Phys.* **2008**, *129*, 084701.
(25) Zhang, J. Z. *J. Phys. Chem. B* **2000**, *104*, 7239.
(26) Ueda, A.; Tayagaki, T.; Kanemitsu, Y. *J. Phys. Soc. Jpn.* **2009**, *78*, 083706.
(27) Klimov, V. I.; McGuire, J. A.; Schaller, R. D.; Rupasov, V. I. *Phys. Rev. B* **2008**, *77*, 195324.
(28) Barzykin, A. V.; Tachiya, M. *J. Phys.: Condens. Matter* **2007**, *19*, 065105.
(29) Hefetz, Y.; Goltsos, W. C.; Nurmikko, A. V.; Kolodziejski, L. A.; Gunshor, R. L. *Appl. Phys. Lett.* **1986**, *48*, 372.
(30) Seufert, J.; Bacher, G.; Scheibner, M.; Forchel, A.; Lee, S.; Dobrowolska, M.; Furdyna, J. K. *Phys. Rev. Lett.* **2001**, *88*, 027402.
(31) $1/\tau_2 = 1/\tau_1 + \langle n_{Mn} \rangle / \tau_{ET}$, where τ_1 and τ_2 are the first order decay time constants of undoped and Mn-doped CdS/ZnS nanocrystals at early delay time (<10 ps).

JP100352M